Analysis and Comparison of Isolated High-Gain High-Voltage DC/DC Converters for Offshore Wind Farm Collection and Integration

Yanan Ye, *Graduate Student Member, IEEE*, Xiaotian Zhang, *Senior Member, IEEE*, Chong Gao, *Student Member, IEEE*, Xianwei Wang, Yue Wang, *Senior Member, IEEE*, and Xu Yang, *Senior Member, IEEE*

***Abstract*—With the vigorous development of offshore wind energy, two-stage voltage step-up HVdc transmission has become a better choice compared with other transmission methods due to the lower cost and higher efficiency. It is essential to step-up the medium voltage (MV) level at the collection grid to the high voltage (HV) level at the export line. Therefore, the research on HV dc/dc converters has received widespread attention. This article introduces two modular multilevel dc/dc converters with high gain, HV, and galvanic isolation, which can be applied to connect the MVdc grid and HVdc grid in offshore wind energy systems. The topologies, operation principles, and control strategies of the two converters are illustrated in the article. The simulation based on power systems computer aided design/electromagnetic transients including DC (PSCAD/EMTDC) and hardware in loop experiment based on real-time digital simulation (RTDS) is completed. The operation principle and control strategy are validated by the simulation results and experiment results. The comparison results in terms of current stresses, costs, and power losses between these two converters and the two representative topologies previously proposed are presented. Then, the overall performance of each topology is evaluated based on the comparison results.**

***Index Terms*—High voltage (HV) dc/dc converter, HVdc grid, medium voltage dc (MVdc) grid, offshore wind energy system.**

I. Introduction

With the rapid consumption of traditional energy and the urgent demand for environmental protection, clean energy, especially offshore wind energy, is gradually becoming a new choice and obtaining increasing attention. Compared with the onshore wind farms, the offshore wind energy resources are more abundant and it is easier to choose the location for construction. Besides, the power generated by offshore wind farms is higher and more stable. Nowadays, the offshore wind power projects are gradually moving toward deep seas to obtain more wind energy resources [1], [2], [3]. However, the long transmission distances make power transmission challenging. Consequently, it is essential to choose appropriate schemes to realize the power collection and integration of the offshore wind energy [4], [5].

Generally, there are mainly two feasible schemes for the transmission of wind energy: high voltage ac (HVac) transmission and HVdc transmission [6], [7], [8]. As the distance of power transmission increases, it is necessary to add reactive power compensation equipment, which will increase the cost of HVac transmission. The optimal transmission distance of traditional HVac transmission is approximately 70–80 km [9]. Therefore, the HVdc transmission will be a better choice for the power transmission when the offshore wind farms are very far away from the land [10], [11], [12].

In the HVdc transmission system, the ac voltage generated by the turbines should be converted into HVdc voltage to increase transmission power and efficiency. Normally, according to the different ways to obtain the high dc voltage, several different kinds of system configurations have been proposed at present [13], [14]. Nevertheless, the ac/ac conversion requires the bulky fundamental-frequency transformers, which will increase the cost of offshore platforms. Thus, the pure dc transmission has better application prospects in future offshore wind power transmission. In particular, the two-stage dc voltage step-up topology is more realistic than the other topologies of pure dc systems [15].

The basic scheme of two-stage dc voltage step-up topology for offshore wind farms is presented in Fig. 1. First, the wind turbine generates the ac voltage and the associated rectifier converts the ac voltage to low voltage dc (LVdc) voltage. Then, the LVdc voltage is boosted to HVdc voltage through two-stage voltage conversion. In the first stage, the intermediate medium voltage (MV) dc/dc converter boosts LVdc voltage to MVdc voltage. In the second stage, the HV dc/dc converter is applied to step-up the MVdc voltage to the HVdc voltage. Finally, the power is

Manuscript received 12 September 2023; revised 15 November 2023; accepted 21 December 2023. Date of publication 27 December 2023; date of current version 16 May 2024. This work was supported by the China Southern Power Grid Company, Ltd., Science and Technology Project: Research on Insulation Design and Parasitic Parameter Optimization Technology for High Voltage SiC Devices and Development of Half Bridge Device Packaging under Grant 030400KC23090015 and Grant GDKIXM20231031. Recommended for publication by Associate Editor Kosala Gunawardane. *(Corresponding author: Xiaotian Zhang.)*

Yanan Ye, Xiaotian Zhang, Chong Gao, Yue Wang, and Xu Yang are with the Department of Electrical Engineering, Xi'an Jiaotong University, Xi'an 710049, China (e-mail: yeyanan@stu.xjtu.edu.cn; xiaotian@xjtu.edu.cn; 3121304401@stu.xjtu.edu.cn; davidwangyue@mail.xjtu.edu.cn; yangxu@mail.xjtu.edu.cn).

Xianwei Wang is with Xi'an XJ Power Electronics Technology Company Ltd., Xi'an 710049, China (e-mail: wangxianwei.xj@cee.com.cn).

Color versions of one or more figures in this article are available at https://doi.org/10.1109/TPEL.2023.3347625.

Digital Object Identifier 10.1109/TPEL.2023.3347625

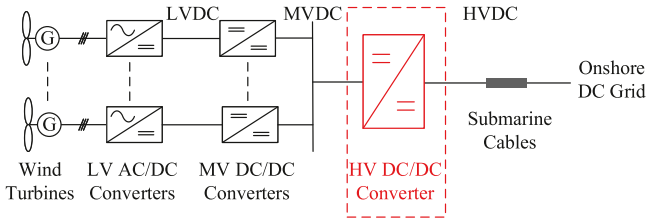

Fig. 1. Basic scheme of two-stage DC voltage step-up topology for offshore wind farms.

transferred from the offshore grid to the onshore grid via the submarine cables.

As one of the key equipment for the offshore wind energy system, the HV dc/dc converter has received lots of attention. Generally, there are several requirements for these converters, given as follows.

1) Galvanic isolation.
2) Bidirectional power transmission.
3) Large voltage step ratio.
4) High power.
5) Low costs and low power losses.

In the last decades, many scholars have working on HV dc/dc converter and lots of topologies have been proposed. Due to the advantages of scalability and modular structure, the isolated dc/dc converter topologies based on modular multilevel converter (MMC) have been proposed [16], [17], [18]. To reduce the costs, the nonisolated dc/dc converter topologies based on MMC are introduced [19], [20], [21], [22], [23]. The hybrid topologies based on MMC replace some submodules (SMs) with transistor valves, which can significantly reduce the costs and power losses [24], [25], [26]. In the meantime, lots of topologies using dual active bridge (DAB) or single active bridge (SAB) as the converter units are proposed [27], [28], [29], [30], [31], [32]. They change the terminal voltage and voltage step ratio through different connection configurations of many converter units. A number of topologies combine the MMC and DAB/SAB together [33], [34], [35], [36], [37], and [38]. They can reduce the number of isolated transformers and can easily realize the high-voltage step ratio. Furthermore, several topologies utilize dc choppers instead of DABs as converter units to avoid the use of transformers. Therefore, to achieve better technical and economic benefits, the analysis and comparison of the typical HV dc/dc converter topologies are essential.

This article aims to solve the problem of how to choose an HV dc/dc converter in offshore wind energy transmission systems. It introduces two possible schemes of the HV dc/dc converters, which have the characteristics of high voltage, high power, and high gain. Then, the two topologies are compared with the other two representative topologies previously proposed in terms of current stresses, costs, and efficiencies. Based on the comparison results, this article provides ideas and suggestions for the design and selection of HV dc/dc converters in offshore wind energy transmission systems.

The rest of this article is organized as follows. The topologies, operation principles, and control strategies of the two dc/dc converters are described in Section II. The simulation results and the experiment results are presented in Section III. The theoretical analysis and comparison results of the four topologies are illustrated in Section IV. Finally, Section V concludes this article.

II. Two Possible Schemes

A. Scheme A

1) Topology: The topology of the dc/dc converter in Scheme A is shown in Fig. 2. This dc/dc converter is composed of $2N$ dc/dc converter units and the connection architecture is shown in Fig. 2(a). The circuit of a single dc/dc converter unit is shown in Fig. 2(b).

Each unit consists of three parts: the primary side, the transformer, and the secondary side. The circuit on the primary side is a neutral-point-clamped (NPC) circuit, which contains two dc-link capacitors (C_{in0} and C_{in1}), four diodes (D_1, D_2, ... and D_4) and eight insulated gate bipolar transistor (IGBT) (S_1, S_2, ... and S_8). The circuit on the secondary side contains two dc-link capacitors (C_{out0} and C_{out1}) and two arms. As shown in Fig. 2(c), each arm consists of an arm inductor (L_a) and a stack. The stack is composed of several series-connected SMs (SM_1, SM_2, ... and SM_k), which can be half-bridge submodules (HBSMs) or full-bridge submodules (FBSMs). The circuit on the primary side and the secondary side both perform as dc/ac converters and they are connected via the isolated transformer (T_a). The turn ratio of the transformer is $1:\gamma_T$, and the leakage inductance is L_T.

2) Operation Principles: To illustrate the operation principles of this dc/dc converter, the waveforms of ac voltage (v_p) on the primary side, the ac voltage (v_s) on the secondary side, and the current (i_L) flowing through the leakage inductor (L_T) are shown in Fig. 3. The ac voltage v_p is the square wave voltage, which is generated by the NPC circuit on the primary side. The IGBTs in the same leg are turned ON or OFF at the same time. The ac voltage v_s is the trapezoidal wave voltage, which is generated by the multilevel modular converter on the secondary side. The periods of v_p and v_s are both T_s. There is a phase shift (D) between the v_p and v_s, and the voltage stepped transition period is $d \cdot T_s$.

The quasi-two-level (Q2L) modulation (also known as the trapezoidal or quasi-square waveform modulation) is adopted for the multilevel modular converter on the secondary side [39]. When the square wave voltage changes, the slope of square wave voltage is reduced by introducing different voltages so that the output voltage is similar to the trapezoidal waveform. Under the same operation condition, it can reduce the sizes of passive components and the power losses compared with the sinusoidal modulation, and it can significantly reduce the dv/dt stresses compared with the two-level modulation [40], [41].

In order to maximize the utilization of devices, the modulation indexes of all the arms are all one. Therefore, the amplitude (V_p) of v_p and the amplitude (V_s) of v_s can be obtained

$$V_p = V_{\text{in}}, \qquad V_s = \frac{1}{2}V_{\text{out}}. \tag{1}$$

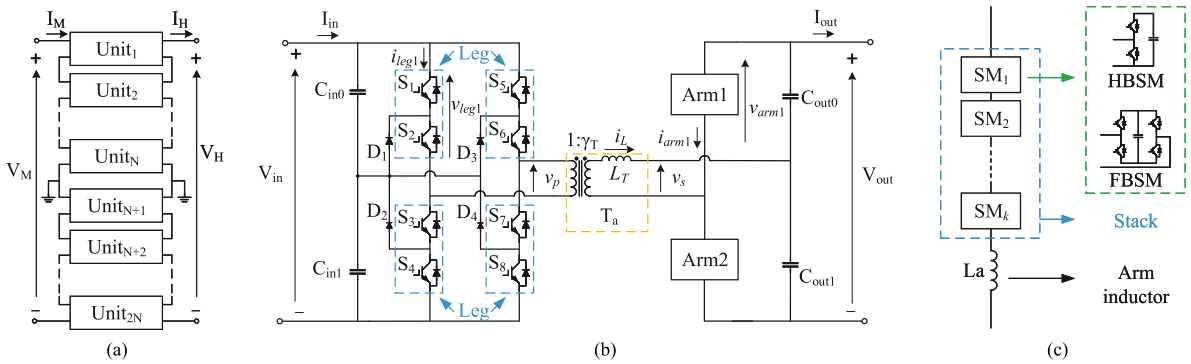

Fig. 2. Topology of the DC/DC converter in Scheme A. (a) Connection architecture of DC/DC converter units. (b) Circuit of single DC/DC converter unit. (c) Structure of an arm.

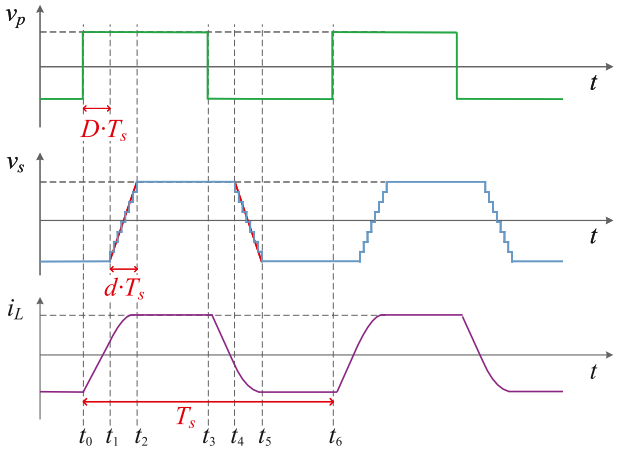

Fig. 3. Operation principles of the DC/DC converter in Scheme A.

Then, the v_p and v_s can be obtained as

$$v_p(t) = \begin{cases} \frac{1}{2}V_{\text{in}} & t_0 \le t < t_3 \\ -\frac{1}{2}V_{\text{in}} & t_3 \le t < t_6 \end{cases} \tag{2}$$

$$v_s(t) = \begin{cases} -\frac{1}{2}V_{\text{out}} & t_0 \le t < t_1, \quad t_5 \le t < t_6 \\ -\frac{1}{2}V_{\text{out}} + \frac{V_{\text{out}}}{dTs}(t - t_1) & t_1 \le t < t_2 \\ \frac{1}{2}V_{\text{out}} & t_2 \le t < t_4 \\ \frac{1}{2}V_{\text{out}} - \frac{V_{\text{out}}}{dTs}(t - t_4) & t_4 \le t < t_5. \end{cases} \tag{3}$$

Thus, the turn ratio γ_T of the isolated transformer and the voltage ratio γ_u of each unit can be obtained as

$$\gamma_T = \frac{V_s}{V_p} = \frac{V_{\text{out}}}{2V_{\text{in}}} \tag{4}$$

$$\gamma_u = \frac{V_{\text{out}}}{V_{\text{in}}} = 2\gamma_T. \tag{5}$$

Considering the connection architecture of the units, the voltage ratio of the dc/dc converter in Scheme A can be obtained as

$$\gamma = \frac{V_H}{V_M} = \gamma_u = 2\gamma_T. \tag{6}$$

According to (2) and (3), the i_L can be got as

$$i_L(t) = \frac{1}{L}\int_{t0}^{t} [v_p(t) - v_s(t)]dt + i_L(t_0). \tag{7}$$

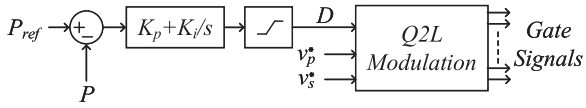

Fig. 4. Control strategy of the DC/DC converter in Scheme A.

Then, the power P_u of the dc/dc converter unit and the power P of the dc/dc converter in Scheme A can be calculated as

$$\begin{aligned} P_u &= \frac{1}{T_s}\int_{t_0}^{t_6} i_L(t) \cdot v_p(t)dt \\ &= \frac{\gamma_T V_{\text{in}} V_{\text{out}}}{12Lf_s}(12D^2 + 4d^2 + 12Dd - 6D - 3d) \end{aligned} \tag{8}$$

$$\begin{aligned} P &= 2NP_u \\ &= \frac{{\gamma_T}^2 {V_M}^2}{12NLf_s}(12D^2 + 4d^2 + 12Dd - 6D - 3d). \end{aligned} \tag{9}$$

It can be seen that the power of the dc/dc converter is related to the terminal voltages, the leakage inductance of the transformer, the ac operation frequency, the phase shift, and the voltage stepped transition period. Generally, the voltage stepped transition period is constant and the power can be regulated by changing the phase shift (D) in the controller. The leakage inductance of the transformer determines the maximum power, which can be used to design the parameters of the dc/dc converter.

3) Control Strategy: The control strategy of the dc/dc converter in Scheme A is shown in Fig. 7. The power is regulated by adjusting the phase shift (D) between the ac voltage (v_p) on the primary side and the ac voltage (v_s) on the secondary side. The proportional-integral (PI) controller is used to regulate the power of the dc/dc converter in a feedback manner. The gate signals of the semiconductor switches are generated via the Q2L modulation.

B. Scheme B

1) Topology: The topology of the dc/dc converter in Scheme B, which is composed of $2N$ dc/dc converter units, is shown in Fig. 5. Fig. 5(a) shows the connection architecture of the units, and Fig. 5(b) shows the circuit of a single unit.

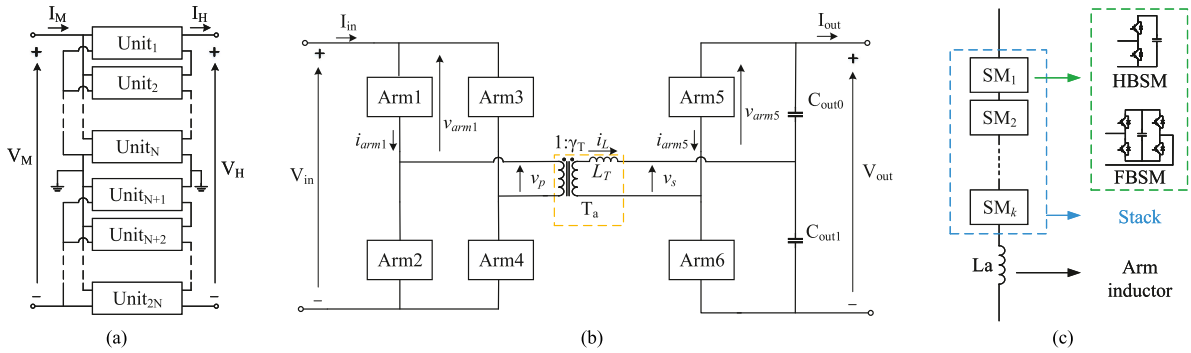

Fig. 5. Topology of the DC/DC converter in Scheme B. (a) Connection architecture of the DC/DC converter units. (b) Circuit of a single DC/DC converter unit. (c) Structure of an arm.

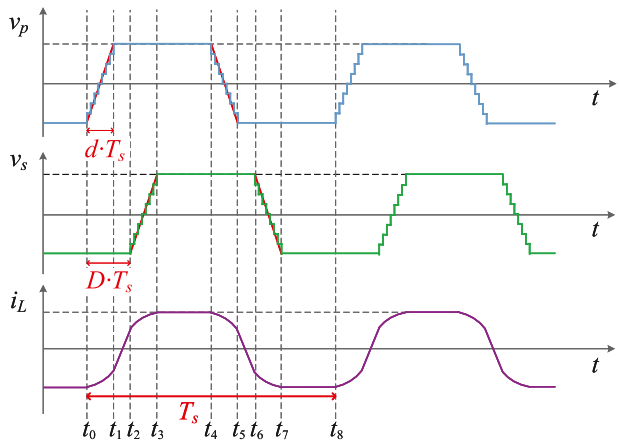

Fig. 6. Operation principles of the DC/DC converter unit in Scheme B.

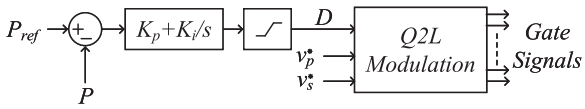

Fig. 7. Control strategy of the DC/DC converter in Scheme B.

Similar to the dc/dc converter unit in Scheme A, each unit consists of the primary side, the transformer, and the secondary side. The circuit on the primary side contains four arms and the circuit on the secondary side is composed of two dc-link capacitors and two arms. The isolated transformer (T_a) is used to connect the primary side and the secondary side. The turn ratio is $1:\gamma_T$, and the leakage inductance is L_T.

2) Operation Principles: Fig. 6 shows the waveforms of the ac voltage (v_p) on the primary side, the ac voltage (v_s) on the secondary side, and the current (i_L) flowing through the inductor (L_T). Since the circuits on the primary side and the secondary side are both multilevel modular dc/ac converters, the ac voltages v_p and v_s are both trapezoidal wave voltages. The quasi-square-wave modulation is adopted for the multilevel modular converter on both two sides. Similarly, the modulation indexes of the arms are all one to maximize the utilization of devices. Therefore, the amplitude (V_p) of v_p and the amplitude (V_s) of v_s can be obtained

$$V_p = V_{\text{in}}, \qquad V_s = \frac{1}{2}V_{\text{out}}. \tag{10}$$

Then, the v_p and v_s can be obtained as

$$v_p(t) = \begin{cases} -\frac{1}{2}V_{\text{in}} + \frac{V_{\text{in}}}{d\cdot Ts}(t-t_0) & t_0 \le t < t_1 \\ \frac{1}{2}V_{\text{in}} & t_1 \le t < t_4 \\ \frac{1}{2}V_{\text{in}} - \frac{V_{\text{in}}}{d\cdot Ts}(t-t_4) & t_4 \le t < t_5 \\ -\frac{1}{2}V_{\text{in}} & t_5 \le t < t_8 \end{cases} \tag{11}$$

$$v_s(t) = \begin{cases} -\frac{1}{2}V_{\text{out}} + \frac{V_{\text{out}}}{d\cdot Ts}(t-t_2) & t_2 \le t < t_3 \\ \frac{1}{2}V_{\text{out}} & t_3 \le t < t_6 \\ \frac{1}{2}V_{\text{out}} - \frac{V_{\text{out}}}{d\cdot Ts}(t-t_6) & t_6 \le t < t_7 \\ -\frac{1}{2}V_{\text{out}} \quad t_0 \le t < t_2, & t_7 \le t < t_8. \end{cases} \tag{12}$$

Thus, the turn ratio γ_T of the isolated transformer and the voltage ratio γ_u of each unit can be obtained as

$$\gamma_T = \frac{V_s}{V_p} = \frac{V_{\text{out}}}{2V_{\text{in}}} \tag{13}$$

$$\gamma_u = \frac{V_{\text{out}}}{V_{\text{in}}} = 2\gamma_T. \tag{14}$$

Considering the connection architecture, the voltage ratio of the dc/dc converter can be obtained as

$$\gamma = \frac{V_H}{V_M} = N\cdot\gamma_u = 2N\gamma_T. \tag{15}$$

According to (11) and (12), the i_L can be got as

$$i_L(t) = \frac{1}{L}\int_{t0}^{t}[v_p(t) - v_s(t)]dt + i_L(t_0). \tag{16}$$

Then, the power P_u of dc/dc converter unit and the power P of dc/dc converter in Scheme B can be calculated as

$$\begin{aligned} P_u &= \frac{1}{T_s}\int_{t_0}^{t_8} i_L(t)\cdot v_p(t)dt \\ &= \frac{\gamma_T V_{\text{in}} V_{\text{out}}}{6Lf_s}[3D(1-2D) - d^2] \end{aligned} \tag{17}$$

$$\begin{aligned} P &= 2NP_u \\ &= \frac{N\gamma_T^2 {V_M}^2}{6Lf_s}[3D(1-2D) - d^2]. \end{aligned} \tag{18}$$

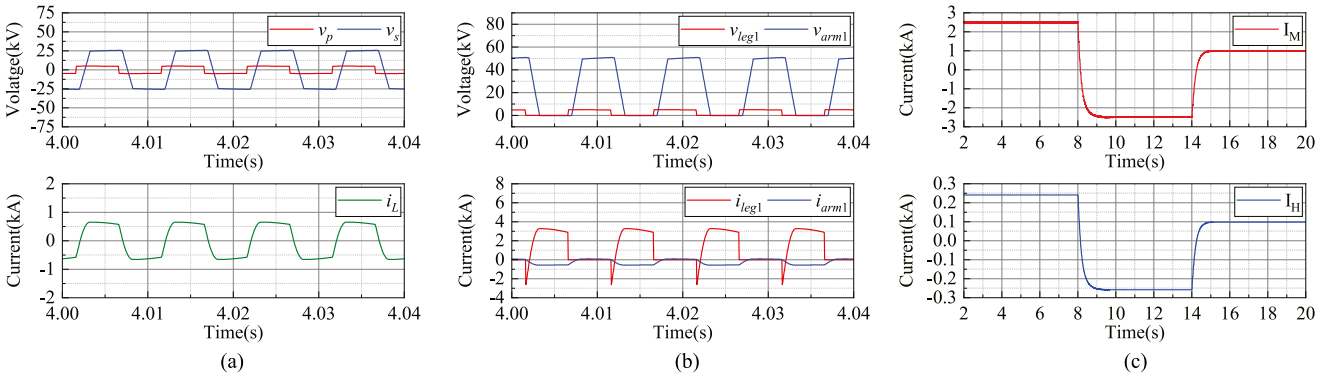

Fig. 8. Simulation results of DC/DC converter in Scheme A. (a) AC voltages (v_p), AC voltages (v_s), and the AC current (i_L). (b) Voltages and currents of the Leg1 and Arm1. (c) Terminal currents of the DC/DC converter.

TABLE I
PARAMETERS OF THE HV DC/DC CONVERTER IN THE OFFSHORE WIND ENERGY SYSTEM

Symbol	Description	Value
V_H	HVdc terminal voltage	$\pm$200 kV
V_M	MVdc terminal voltage	$\pm$20 kV
P	Rating power	100 MW

TABLE II
SIMULATION PARAMETERS OF DC/DC CONVERTER IN SCHEME A

Symbol	Description	Value
$2N$	Number of units	8
V_{in}	Input voltage of single unit	5 kV
V_{out}	Output voltage of single unit	50 kV
P_u	Rating power of single unit	12.5 MW
Np	Number of IGBTs in each leg on the primary side	2
Ns	Number of SMs in each arm on the secondary side	25
γ_T	Turn ratio of isolated transformer	1 : 5

Similar to the dc/dc converter in Scheme A, the power can be regulated by changing the phase shift in the controller. The leakage inductance of the transformer can be designed according to the rated power or maximum power of this dc/dc converter.

3) Control Strategy: The control strategy of the dc/dc converter in Scheme B is shown in Fig. 7. The power is regulated by adjusting the phase shift (D) between the ac voltage (v_p) on the primary side and the ac voltage (v_s) on the secondary side. Similar to Scheme A, the power of the dc/dc converter in Scheme B is regulated via a PI controller. The gate signals of the semiconductor switches are also generated by the Q2L modulation.

III. SIMULATION AND EXPERIMENT

A. Case Study

To complete the analysis and comparison of the different HV dc/dc converter topologies, this section takes a typical offshore wind energy system as a study case. The structure of this energy transmission system is the same, as shown in Fig. 1. The basic parameters of the HV dc/dc converter connecting the HVdc side and MVdc side in this system are given in Table I. The voltage on HVdc side is $\pm$200 kV, and the voltage on MVdc side is $\pm$20 kV. The rating power of the dc/dc converter is 100 MW and it is required to realize the bidirectional power transmission. In order to improve the reliability of this energy transmission system, it is essential to realize the galvanic isolation between the HVdc side and MVdc side in this system.

TABLE III
SIMULATION PARAMETERS OF DC/DC CONVERTER IN SCHEME B

Symbol	Description	Value
$2N$	Number of units	10
V_{in}	Input voltage of single unit	20 kV
V_{out}	Output voltage of single unit	40 kV
P_u	Rating power of single unit	10 MW
Np	Number of SMs in each arm on the primary side	10
Ns	Number of SMs in each arm on the secondary side	20
γ_T	Turn ratio of isolated transformer	1 : 1

B. Simulation Results

The models of the two presented dc/dc converters in Schemes A and B are built in PSCAD/EMTDC to verify the operation principles and control strategies. The topologies of the two HV dc/dc converters are shown in Figs. 2 and 5. The detailed parameters are given in Tables II and III. The simulation results are shown in Figs. 8 and 9.

Fig. 8(a) shows the ac voltages (v_p and v_s) on both sides of the isolated transformer and the current (i_L) flowing through the leakage inductor of the dc/dc converter unit in Scheme A. It can be seen that the v_p is a square waveform voltage with the amplitude of 5 kV and the v_s is a trapezoidal waveform voltage with the amplitude of 25 kV. The periods of the ac voltages and ac currents are all $T_s = 10$ ms and the voltage stepped transition period is $d \cdot T_s = 1.25$ ms.

Fig. 8(b) shows the leg voltage and current (v_{leg1} and i_{leg1}) on the primary side and the arm voltage and current (v_{arm1} and i_{arm1}) on the secondary side of the dc/dc converter unit in Scheme A. It can be seen that the v_{leg1} is square waveform and the voltage is changed between 0 and 5 kV. The v_{arm1} is trapezoidal waveform and the voltage is changed between 0 and 50 kV. The i_{leg1} and i_{arm1} are both ac currents with dc offset. The dc current component of the i_{leg1} is positive and the dc current component

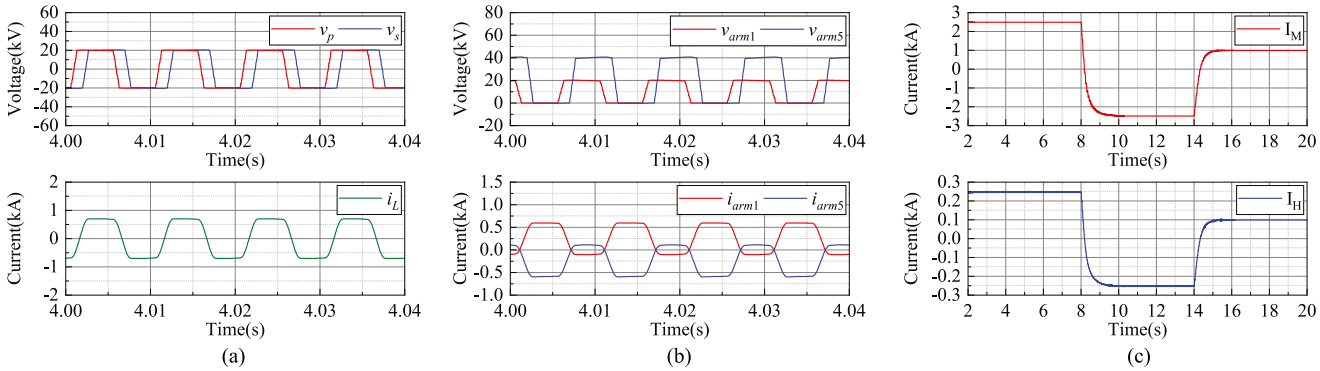

Fig. 9. Simulation results of the DC/DC converter in Scheme B. (a) AC voltages (v_p), AC voltages (v_s), and the AC current (i_L). (b) Voltages and currents of the Arm1 and Arm5. (c) Terminal currents of the DC/DC converter.

of the i_{arm1} is negative, which means that the power is transferred from the MVdc side to the HVdc side.

Fig. 8(c) shows the terminal currents (I_H and I_M) of the dc/dc converter in Scheme A. The terminal current I_M changes from 2.5 to -2.5 kA at 8 s and changes from -2.5 to 1 kA at 14 s. It can be seen that the terminal currents of the dc/dc converter in Scheme A both have very small ripples under steady states and have good dynamic response performance. Meanwhile, the bidirectional power transmission is realized.

Fig. 9(a) shows the ac voltages (v_p and v_s) on both sides of the isolated transformer and the current (i_L) flowing through the leakage inductor in Scheme B. It can be seen that the v_p and v_s are both trapezoidal waveforms and the amplitudes are both 20 kV. The periods of ac voltages and ac current are all $T_s = 10$ ms and the voltage stepped transition period is $d \cdot T_s = 0.72$ ms.

Fig. 9(b) shows the arm voltages and current (v_{arm1} and i_{arm1}) on the primary side of the dc/dc converter unit, as well as the arm voltages and current (v_{arm5} and i_{arm5}) on the secondary side in Scheme B. It can be seen that the v_{arm1} is a trapezoidal waveform and the voltage is changed between 0 and 40 kV. The v_{arm5} is also a trapezoidal waveform and the voltage is changed between 0 and 20 kV. The dc current component of the i_{arm1} is positive and the dc current component of the i_{arm5} is negative, which means that the power is transferred from the MVdc side to the HVdc side.

Fig. 9(c) shows the terminal currents (I_H and I_M) of the dc/dc converter in Scheme B. The terminal current (I_M) on the MVdc side changes from 2.5 to -2.5 kA at 8 s and changes from -2.5 to 1 kA at 14 s. It can be seen that the dc/dc converter in Scheme B also has good performance in both steady state and dynamic response.

C. Experiment Results

Apart from the theoretical analysis and simulation results, the hardware in loop (HIL) experimental systems based on the RTDS platform are built to verify the operation principles and control strategies of dc/dc converters in the two schemes. The structure and the prototype of the experiment platform are shown in Fig. 12. Due to the limitation of the laboratory equipment, compared with the bipolar dc power transmission system built in simulation, a monopolar system is built in the HIL experiment systems. The parameters of the two dc/dc converters are the same as those in the simulation.

The experiment results of Schemes A and B are shown in Figs. 10 and 11, respectively. Since there are parasitic parameters of the semiconductor switches, the arm voltages in the experiment are not perfect square or trapezoidal waves. Nevertheless, it can be seen that the experiment results are basically consistent with the simulation results. The topologies, operation principles, and control strategies of the two schemes are validated by the experiment tests.

IV. Comparison

To demonstrate the advantages and characteristics of the two schemes presented in this article, they are compared with the other two schemes proposed previously based on current stresses, costs, and efficiencies in this section. All the dc/dc converters are analyzed and compared under the same condition when the parameters of the wind energy transmission system are set in Table I.

The topologies of the dc/dc converters in Schemes C and D are shown in Figs. 13 and 14, separately [17], [29]. The dc/dc converter in Scheme C (as shown in Fig. 13) is composed of ten units ($N = 5$), and the connection architecture is shown in Fig. 13(a). The topology of a single dc/dc converter unit is shown in Fig. 13(b) and each unit also consists of three parts: the primary side, the transformer, and the secondary side. The primary side contains two parts, which are parallel connected. The circuit on each part consists of four arms and each arm contains ten HBSMs. The circuit on the secondary side is composed of four arms and each arm contains 20 HBSMs. The primary side and the secondary side are connected via an isolated three-windings transformer whose ratio is $1:1:\gamma_T = 1:1:2$. The dc/dc converter in Scheme D (as shown in Fig. 13) is composed of 20 units ($N = 10$), and the connection architecture is shown in Fig. 14(a). The topology of a single dc/dc converter unit is shown in Fig. 14(b) and each unit is composed of ten DABs ($m = 10$),

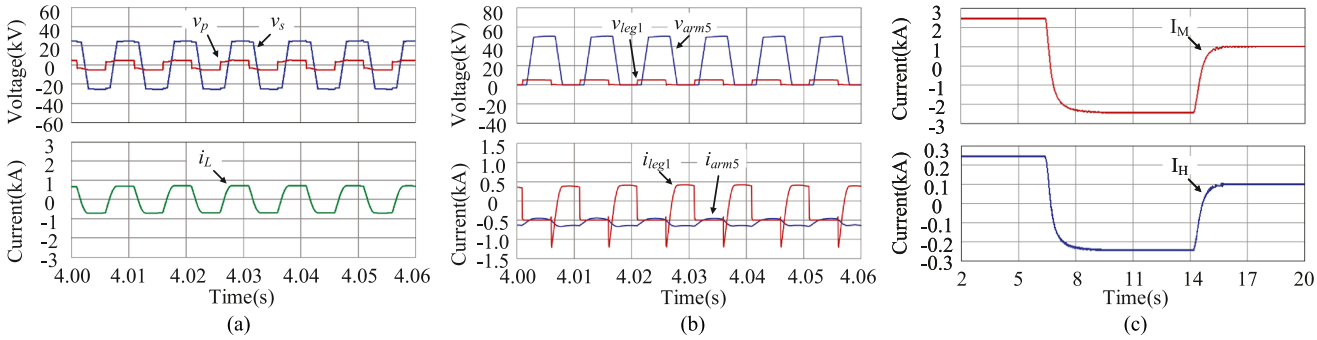

Fig. 10. Experiment results of DC/DC converter in Scheme A. (a) AC voltages (v_p), AC voltages (v_s), and the AC current (i_L). (b) Voltages and currents of the Leg1 and Arm1. (c) Terminal currents of the DC/DC converter.

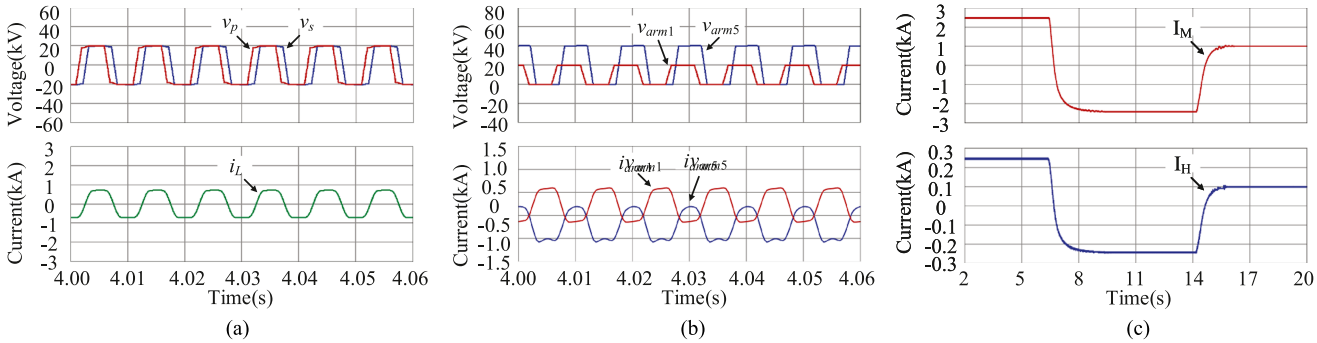

Fig. 11. Experiment results of DC/DC converter in Scheme B. (a) AC voltages (v_p), AC voltages (v_s), and the AC current (i_L). (b) Voltages and currents of the Arm1 and Arm5. (c) Terminal currents of the DC/DC converter.

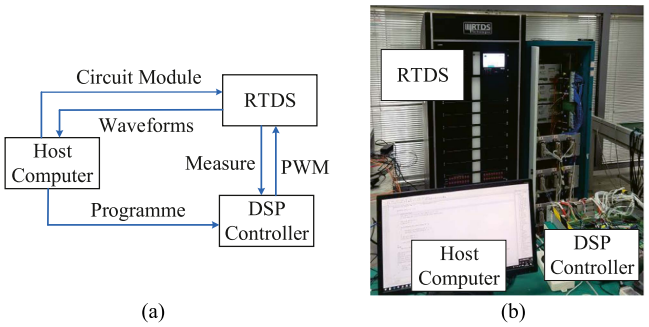

Fig. 12. Experiment platform. (a) Structure of the experiment platform. (b) Prototype of the experiment platform.

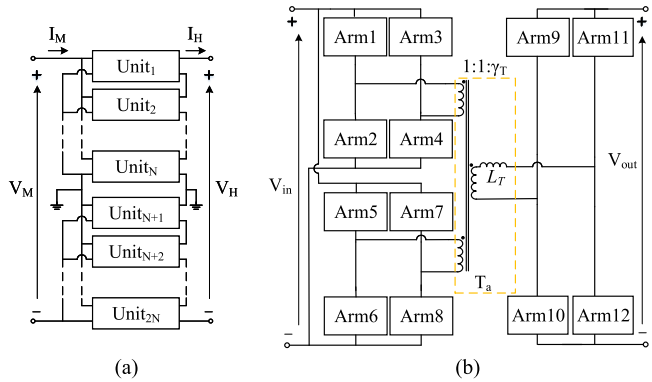

Fig. 13. Topology of the DC/DC converter in Scheme C. (a) Connection architecture of the DC/DC converter units. (b) Circuit of the single DC/DC converter unit.

which are input-parallel-output-series connected. The turn ratio of the isolated transformer in each DAB is $1:\gamma_T = 1:1$.

A. Semiconductor Switches

It is essential to calculate the current stresses of the switches to select the proper semiconductor devices. The isolated dc/dc converters are generally composed of dc/ac converters. The calculation methods of the current stresses are different when the structures are different. There are four typical structures of dc/ac converters, which are shown in Fig. 15.

If the converter is a half-bridge structure and consists of series connected SMs [see Fig. 15(a)], the maximum value ($\hat{i}_{\text{arm}}$) of arm currents can be obtained as

$$\hat{i}_{\text{arm}} = I_{\text{dc}} + \frac{1}{2}\hat{i}_{\text{ac}} \tag{19}$$

where $\hat{i}_{\text{ac}}$ is the maximum value of ac current.

If the converter is a full-bridge structure and consists of series connected SMs [see Fig. 15(b)], the maximum value ($\hat{i}_{\text{arm}}$) of arm currents can be obtained as

$$\hat{i}_{\text{arm}} = \frac{1}{2}I_{\text{dc}} + \frac{1}{2}\hat{i}_{\text{ac}}. \tag{20}$$

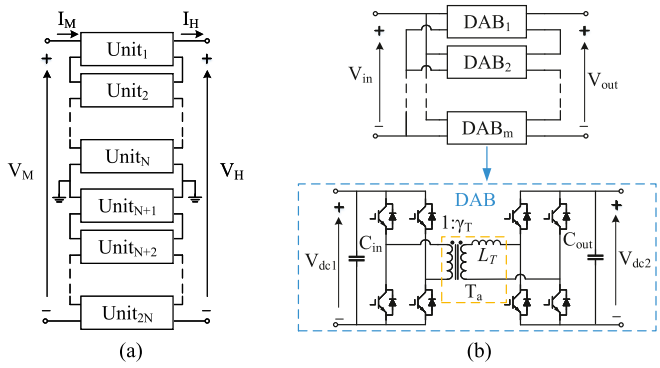

Fig. 14. Topology of the DC/DC converter in Scheme D. (a) Connection architecture of the DC/DC converter units. (b) Circuit of the single DC/DC converter unit.

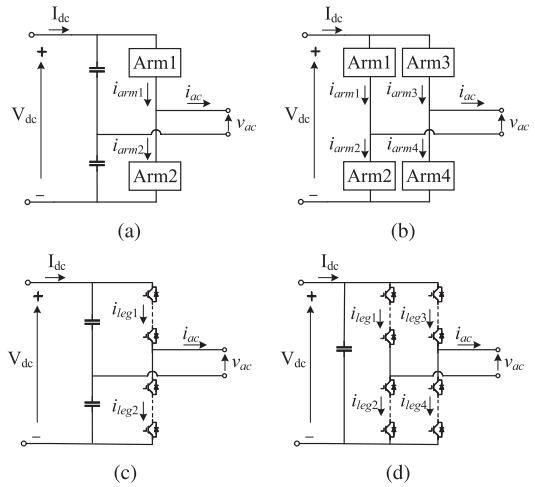

Fig. 15. Four typical structures of the DC/AC converters. (a) Half-bridge structure converter composed of SMs. (b) Full-bridge structure converter composed of SMs. (c) Half-bridge structure converter composed of switches. (d) Full-bridge structure converter composed of switches.

If the converter is full-bridge or half-bridge structure and consists of switches [see Fig. 15(c) and (d)], the maximum value ($\hat{i}_{\text{leg}}$) of arm current can be obtained as

$$\hat{i}_{\text{leg}} = \hat{i}_{\text{ac}}. \tag{21}$$

According to the calculation methods, the component current stresses of the dc/dc converters in four schemes are obtained and the results are shown in Fig. 16. In Scheme A, the current stresses of switches on the primary side are 3263 A and those on the secondary side are 576 A. In other schemes, the current stresses of switches on the primary side are equal to those on the secondary side. The current stresses of switches in the other three schemes are 605, 303, and 357 A, respectively.

Normally, the semiconductor switches are selected by the rated voltage and the rated current. A margin will be left to improve the reliability of devices and systems. Since all the IGBTs in the four schemes are required to withstand about 2 kV, the rated collector–emitter voltage is selected as 4.5 kV. Then, according to the current stresses calculated before, the selected

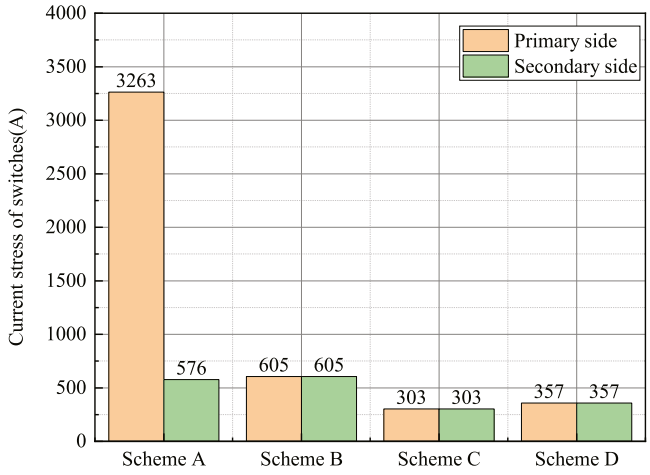

Fig. 16. Current stresses of the switches in the four DC/DC converters.

TABLE IV
SWITCHES SELECTED IN THE FOUR DC/DC CONVERTERS

Items	Primary side	Secondary side
Scheme A	5SNA3000K452300	CM1200HG-90R
Scheme B	CM1200HG-90R	CM1200HG-90R
Scheme C	CM600HG-90H	CM600HG-90H
Scheme D	CM600HG-90H	CM600HG-90H

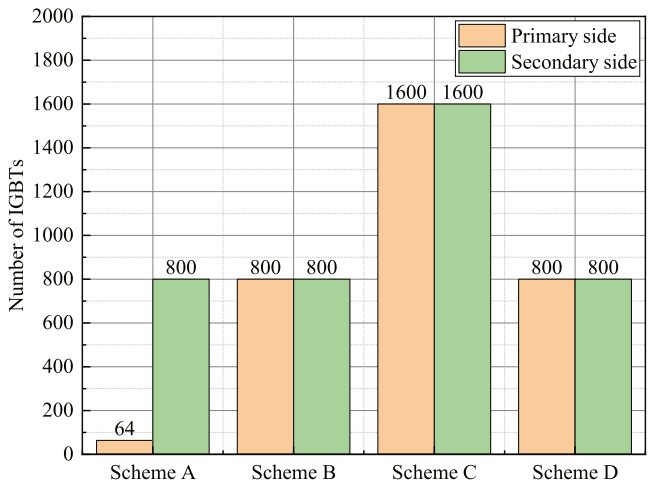

Fig. 17. Number of the switches in the four DC/DC converters.

IGBT types are given in Table IV. For the dc/dc converter in Scheme A, the 5SNA3000K452300 is chosen on the primary side and the CM1200HG-90R is chosen on the secondary side. The CM1200HG-90R is selected for all the switches in Scheme B. Meanwhile, the CM600HG-90H is selected for all the switches in Schemes C and D.

Then, the numbers of IGBTs in the four schemes are calculated separately and the results are shown in Fig. 17. It can be seen that the dc/dc converter in Scheme A requires 864 IGBTs, which contains 800 CM1200HG-90R and 64 5SNA3000K452300. The dc/dc converter in Scheme B requires both 800 CM1200HG-90R for the primary side and

secondary side. The dc/dc converter in Scheme C requires both 1600 CM600HG-90H for the primary side and secondary side. The dc/dc converter in Scheme D requires both 800 CM600HG-90H for the primary side and secondary side.

It can be seen that the current stresses of switches in the dc/dc converters in Schemes A and B are higher than the current stresses of the switches in the other two dc/dc converters. Especially, the current stresses of switches on the primary side of the dc/dc converter in Scheme A are the highest. The component current stresses in Scheme C are the lowest compared with the other three schemes. Due to the different current stresses, the type and the number of semiconductor switches are different. The switches on the secondary side in Scheme A and all switches in Scheme B are the same due to the similar current stresses. Besides, all switches in Schemes C and D are the same. Meanwhile, the number of switches in the dc/dc converter in Scheme A is the lowest compared with the other three schemes. The number of switches in Schemes B and D are the same. The number of semiconductor switches in Scheme C is the highest in the four schemes.

B. Capacitors

To ensure that the dc/dc converter can work well, it is essential to keep the SM capacitor voltages balanced and stable. The SM capacitor voltage balance is realized by the modulation strategy and the SM capacitor voltage ripples are related to the value of capacitance. It is assumed that the SM capacitor voltages in the stacks are balanced well in normal operation. The amount of capacitors used to balance voltage in the stack is N_C and the SM capacitance is $C_{\rm SM}$. The rated SM capacitor voltage is V_C and the ripple of a single capacitor voltage is represented by $v_{C\_\rm ac}(t)$

$$e_{ST}(t) = \frac{1}{2}CN_C[V_C + v_{C\_\rm ac}(t)]^2 = \frac{1}{2}C_{\rm SM}N_C[V_C^2 + 2V_C v_{C\_\rm rip}(t) + v_{C\_\rm ac}^2(t)]. \quad (22)$$

Since the quadratic term of the fluctuation value is too small, it can be neglected. Then, the capacitor voltage ripple can be obtained as

$$v_{C\_\rm ac}(t) = \frac{e_{ST\_\rm ac}(t)}{C_{\rm SM}N_C V_C}. \quad (23)$$

Meanwhile, the ac energy components of stacks can be calculated by the stack power exchange. Then, it can be obtained that

$$e_{ST\_\rm ac}(t) = \int_0^t v_p(t)\cdot i_p(t)\mathrm{d}t. \quad (24)$$

Submitting (24) into (23), the capacitor voltage ripple can be calculated. Then, the fluctuation of SM capacitor voltage is calculated as

$$\xi = \frac{v_{C\_\rm ac\,max} - v_{C\_\rm ac\,min}}{V_C} \quad (25)$$

where $v_{C\_\rm ac\,max}$ and $v_{C\_\rm ac\,min}$ are the maximum value and minimum value of the capacitor voltage ripple, respectively.

TABLE V
PARAMETERS OF THE CAPACITORS

Items	Scheme A			Scheme B		Scheme C	Scheme D
Type	$C_{\rm SM}$	$C_{\rm in}$	$C_{\rm out}$	$C_{\rm SM}$	$C_{\rm out}$	$C_{\rm SM}$	$C_{\rm in}$, $C_{\rm out}$
V_C(kV)	2	2.5	25	2	20	2	2
C(mF)	1.41	5	0.2	1.83	0.2	0.96	5
N_C	400	16	16	800	20	1600	400

note V_C: the rated voltage of capacitors· C : The capacitance of capacitors· N_C : The number of capacitors.

TABLE VI
PARAMETERS OF THE ISOLATED TRANSFORMERS

Items	Scheme A	Scheme B	Scheme C	Scheme D
Vp	25 kV	20 kV	40 kV	2 kV
Vs	5 kV	20 kV	20 kV	2 kV
Vt	–	–	20 kV	–
P_T	12.5 MVA	10 MVA	10 MVA	0.5 MVA
f	100 Hz	100 Hz	100 Hz	500 Hz
N_T	8	10	10	200
Volume	12.5 m^3	12.5 m^3	18.75 m^3	0.75 m^3
Weight	10000 kg	9000 kg	9000 kg	500 kg

note V_p: The rated voltage on the primary side. V_s: The rated voltage on the secondary side. V_t: The rated voltage of third windings. P_T : The rated power. f: The rated ac frequency. N_T : The number of transformers in dc/dc converter.

The fluctuation of capacitor voltage is usually limited within 10%, which is widely accepted for MMC [42]. Then, the capacitance of the SM capacitor can be calculated. The capacitance of input/output capacitor can also be obtained according to the requirement of capacitor voltage fluctuation. Then, the capacitance values of the capacitors in the four schemes are set, as given in Table V. It can be seen that the number of SM capacitors depends on the number of SMs and the number of input/output capacitors ($C_{\rm in}$ and $C_{\rm out}$) depend on the number of dc/dc converter units. There are no SM capacitors in Scheme D, but lots of input/output capacitors ($C_{\rm in}$ and $C_{\rm out}$) are required.

C. Magnetic Devices

The rated parameters (mainly including the rated voltage, rated power, and frequency) of the isolated transformers can affect the size, weight, and cost of the magnetic devices. The rated voltage and amounts of the isolated transformers are selected according to the structures and the rated voltages of the dc/dc converters. The leakage inductance and the frequency of the transformer are influenced by the rated powers of the dc/dc converters and the required SM capacitor voltage ripples.

The detailed parameters of the transformers in the four dc/dc converters are given in the Table VI. The rated voltages on the primary side of the transformers in four schemes are 25, 20, 40, and 2 kV. Only the transformer in Scheme C has three windings, whereas the transformers in the other three schemes have two windings. The voltage step ratios of the transformers in the four schemes are 1 : 5, 1 : 1, 1 : 1 : 2, and 1 : 1, respectively. The rated powers of transformers in the four schemes are 12.5, 10, 10, and 0.5 MVA. The frequency of the transformer in Scheme D is 500 Hz, whereas the frequencies of the transformers in the other three schemes are all 100 Hz.

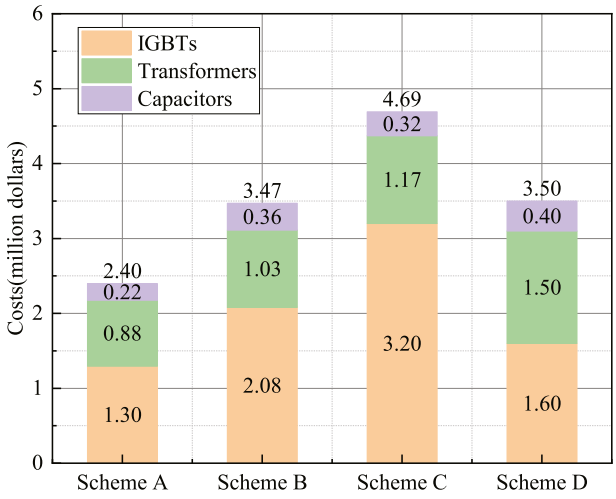

Fig. 18. Costs of the four DC/DC converters.

Then, the costs, volumes, and weights can be estimated by inquiring with suppliers. The total costs of the transformers in four schemes are calculated and the results are shown in Fig. 18. The volumes of each transformer in four schemes are 12.5, 12.5, 18.75, and 0.75m^3. The weights of each transformer in four schemes are 10 000, 9000, 9000, and 500 kg.

It can be seen that the volume and weight of the transformer in Scheme D are the lowest compared with the transformers in the other three schemes due to the lowest voltage, lowest power, and highest frequency. The transformer in Scheme A has the highest turn ratio (1 : 5). The individual transformer in Scheme A has the highest weight because it has the highest power.

D. Cost

In this section, the costs of the four dc/dc converter are calculated and compared. The costs calculated only contain the semiconductor switches, the isolated transformers, and the capacitors (contain C_{SM}, $C_{\text{in}i}$, and $C_{\text{out}i}$). The devices are selected according to the former analysis. The unit prices of various devices are obtained by inquiring with suppliers.

The total costs of the dc/dc converters in four schemes are obtained and the results are shown in Fig. 18. The total costs of the four schemes are 2.38, 3.47, 4.69, and 3.52 million dollars.

It can be seen that the total cost of Scheme A is the lowest, whereas the total cost of Scheme C is the highest. The total costs of Scheme B and Scheme D are basically the same. The costs of the semiconductor switches, transformers, and capacitors in Scheme A are all the least compared with the other three schemes. The total cost of Scheme C is the highest because the costs of semiconductor switches are much higher than the other three schemes. Compared with Scheme D, Scheme B has higher costs of semiconductor switches but lower costs of capacitors and transformers.

E. Efficiency

In this section, the power losses of the four dc/dc converters are calculated and compared. Only the power losses of the semiconductors and power losses of the transformer are considered in this article. Generally, the power losses of the transformer are estimated to be 0.5% of the transformer rated power. However, in this article, the structure of the four dc/dc converters are all isolated, which means that the magnetic losses of the four schemes are the same. Therefore, the magnetic losses of the four schemes are all estimated as 0.5% in the calculation.

The power losses of the semiconductors contain the conductive losses and switching losses [43], [44]. Due to the fact that a single switch or series-connected switches can turn OFF the current, whereas a single SM or series-connected SMs can not, the calculation method for power loss is different.

For the SM, the conducting losses can be calculated as

$$P_{C,T1} = \alpha V_T I_{\text{arm},n,\text{rms}} \tag{26}$$

$$P_{C,D1} = \alpha V_F I_{\text{arm},p,\text{rms}} \tag{27}$$

$$P_{C,T2} = (1-\alpha) V_T I_{\text{arm},p,\text{rms}} \tag{28}$$

$$P_{C,D2} = (1-\alpha) V_F I_{\text{arm},n,\text{rms}} \tag{29}$$

$$P_{C,\text{SM}} = P_{C,T1} + P_{C,D1} + P_{C,T2} + P_{C,D2} \tag{30}$$

where α represents the average duty of the SMs, and the $I_{\text{arm},n,\text{rms}}$ and $I_{\text{arm},n,\text{rms}}$ represent the rms value of arm current when it is positive and when it is negative, respectively.

Then, the switching losses can be calculated as

$$P_{\text{SW},T1} = f_{\text{sw}}(E_{T,\text{ON}} + E_{T,\text{OFF}}) \frac{I_{\text{arm},n,\text{rms}} V_C}{I_{\text{ref}} V_{\text{ref}}} \tag{31}$$

$$P_{\text{SW},D1} = f_{\text{sw}} E_{D,rr} \frac{I_{\text{arm},p,\text{rms}} V_C}{I_{\text{ref}} V_{\text{ref}}} \tag{32}$$

$$P_{\text{SW},T2} = f_{\text{sw}}(E_{T,\text{ON}} + E_{T,\text{OFF}}) \frac{I_{\text{arm},p,\text{rms}} V_C}{I_{\text{ref}} V_{\text{ref}}} \tag{33}$$

$$P_{\text{SW},D2} = f_{\text{sw}} E_{D,rr} \frac{I_{\text{arm},n,\text{rms}} V_C}{I_{\text{ref}} V_{\text{ref}}} \tag{34}$$

$$P_{\text{SW,SM}} = P_{\text{SW},T1} + P_{\text{SW},D1} + P_{\text{SW},T2} + P_{\text{SW},D2} \tag{35}$$

where the I_{ref} and V_{ref} represent the current and voltage under test conditions, respectively.

For the single semiconductor switch, the power losses can be calculated as

$$P_{C,T} = \alpha V_T I_{\text{ac,rms}} \tag{36}$$

$$P_{C,D} = (1-\alpha) V_F I_{\text{ac,rms}} \tag{37}$$

$$P_{\text{SW},T} = f_{\text{sw}}(E_{T,\text{ON}} + E_{T,\text{OFF}}) \frac{I_{\text{ac,rms}} \cdot V_{\text{CE}}}{I_{\text{ref}} V_{\text{ref}}} \tag{38}$$

$$P_{\text{SW},D} = f_{\text{sw}} E_{D,rr} \frac{I_{\text{ac,rms}} \cdot V_{\text{CE}}}{I_{\text{ref}} V_{\text{ref}}} \tag{39}$$

where V_{CE} is the voltage that the switch withstands.

The selection of the IGBT is illustrated in the former section, and the detailed parameters of the IGBTs are given in Table VII. Then, the power losses of the four dc/dc converters are calculated

TABLE VII
DETAILED PARAMETERS OF THE SWITCHES

Parameters	5SNA3000 K452300	CM1200 HG-90R	CM600 HG-90H
Rated collector–emitter voltage, V_{CES}	4.5 kV	4.5 kV	4.5 kV
Rated collector current, I_C	3000 A	1200 A	600 A
Nominal forward voltage of IGBT, V_T	3.65 V	4.4 V	3.7 V
Nominal forward voltage of diode, V_F	3.0 V	2.8 V	4.15 V
Turn-ON energy of IGBT, $E_{T,ON}$	15.5 J	5.1 J	2.8 J
Turn-OFF energy of IGBT, $E_{T,OFF}$	15.1 J	3.85 J	1.7 J
Reverse recovery energy of diode, $E_{D,rr}$	6.7 J	2.1 J	0.67 J

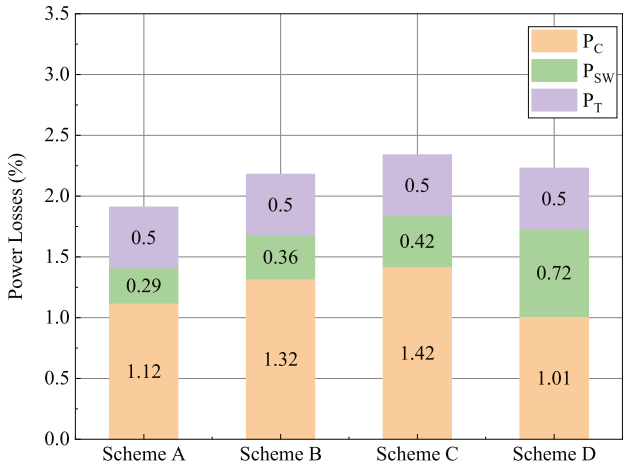

Fig. 19. Power losses of the four DC/DC converters.

and the results are shown in Fig. 19. The total power losses of the four schemes are 1.91%, 2.18%, 2.34%, and 2.23%, respectively. It can be seen that the magnetic losses of the four schemes are all the same because all the power flows through the isolated transformer. Meanwhile, the power losses of the dc/dc converter in Scheme A are the lowest and the power losses of the dc/dc converter in Scheme C are the highest among the four schemes.

In summary, compared with the other two dc/dc converters, the component current stresses in the introduced two dc/dc converters are higher. However, the proposed two schemes have the advantages of lower costs and lower power losses. Especially, the dc/dc converter in Scheme A has the lowest costs and lowest power losses but the highest component current stresses.

The comparison results are summarized as follows.

Scheme A performs well in terms of technology and economy, but has poor reliability. Scheme A has the advantages of fewer semiconductor switches, lower costs, and lower power losses compared with the other three schemes. However, the component current stresses on the primary side are very high. Since each leg on the primary side only contains two semiconductor switches, the damage to every single switch on the primary side will lead to damage to the entire system.

Schemes B and D have similar performance in terms of costs and power losses. The component current stresses in Scheme B are higher than that in Scheme D, resulting in a higher cost of the semiconductor switches in Scheme B than in Scheme D. However, the costs of the capacitors and transformers in Scheme B are both lower than those in Scheme D. As a result, the total cost of Scheme B is only slightly lower than that of Scheme D. Meanwhile, Scheme B has lower switching power losses but higher conducting power losses compared with Scheme D, causing the total power losses of Scheme B to be also only slightly lower than Scheme D.

Scheme C has the highest costs and power losses, but has the lowest component current stresses. Scheme C has the lowest component current stresses compared with the other three schemes, leading to the highest number of semiconductor switches. As a result, the total cost of Scheme C is the highest in the four schemes. Furthermore, the power losses including the conducting losses and the switching losses in Scheme C are higher than those in the other three schemes due to too many semiconductor switches.

V. CONCLUSION

This article introduces two possible high-gain high-voltage dc/dc converter schemes. These two converters are used for the connection of the MVdc side and HVdc side in the offshore wind energy transmission systems. Both of these schemes achieve galvanic isolation in order to improve the reliability of the system. The structures, operation principles, and control strategies of the two converters are presented, and they are verified by the simulation results and experiment results.

A comparison of the two proposed schemes and the other two previous schemes based on current stresses, costs, and efficiencies is completed. There are several conclusions about the comparison results.

1) The costs and power losses of Scheme A are the least, but the reliability is poor.
2) Schemes B and D have similar performance in terms of costs and power losses.
3) Scheme C has the lowest component current stresses but the highest costs and power losses.

Finally, this article also provides ideas for the proposal and selection of future dc/dc conversion schemes for offshore wind energy transmission.

1) Using Q2L modulation can increase the transmission power, improve device utilization, and avoid excessive dv/dt of isolation transformers.
2) The low component current stresses usually lead to high costs and high power losses with the same terminal voltage and transmitted power.
3) In addition to adjusting the turn ratio of the transformer, optimizing the structure of each dc/dc converter unit, and connection architecture the dc/dc converter units can also effectively increase the voltage step ratio of the dc/dc converter.

REFERENCES

[1] J. Liang, T. Jing, O. Gomis-Bellmunt, J. Ekanayake, and N. Jenkins, "Operation and control of multiterminal HVDC transmission for offshore wind farms," *IEEE Trans. Power Del.*, vol. 26, no. 4, pp. 2596–2604, Oct. 2011.

[2] A. Raza, X. Dianguo, S. Xunwen, L. Weixing, and B. W. Williams, "A novel multiterminal VSC-HVdc transmission topology for offshore wind farms," *IEEE Trans. Ind. Appl.*, vol. 53, no. 2, pp. 1316–1325, Mar./Apr. 2017.

[3] A. Egea-Alvarez, F. Bianchi, A. Junyent-Ferre, G. Gross, and O. Gomis-Bellmunt, "Voltage control of multiterminal VSC-HVDC transmission systems for offshore wind power plants: Design and implementation in a scaled platform," *IEEE Trans. Ind. Electron.*, vol. 60, no. 6, pp. 2381–2391, Jun. 2013.

[4] D. Elliott et al., "A comparison of AC and HVDC options for the connection of offshore wind generation in Great Britain," *IEEE Trans. Power Del.*, vol. 31, no. 2, pp. 798–809, Apr. 2016.

[5] L. Yu, R. Li, L. Xu, and G. P. Adam, "Analysis and control of offshore wind farms connected with diode rectifier-based HVDC system," *IEEE Trans. Power Del.*, vol. 35, no. 4, pp. 2049–2059, Aug. 2020.

[6] N. Flourentzou, V. G. Agelidis, and G. D. Demetriades, "VSC-Based HVDC power transmission systems: An overview," *IEEE Trans. Power Electron.*, vol. 24, no. 3, pp. 592–602, Mar. 2009.

[7] D. Jovcic, D. v. Hertem, K. Linden, J.-P. Taisne, and W. Grieshaber, "Feasibility of DC transmission networks," in *Proc. IEEE 2nd PES Int. Conf. Exhib. Innov. Smart Grid Technol.*, 2011, pp. 1–8.

[8] A. Nami, J. Liang, F. Dijkhuizen, and G. D. Demetriades, "Modular multilevel converters for HVDC applications: Review on converter cells and functionalities," *IEEE Trans. Power Electron.*, vol. 30, no. 1, pp. 18–36, Jan. 2015.

[9] Y. Fu, Y. Liu, L.-l. Huang, F. Ying, and F. Li, "Collection system topology for deep-sea offshore wind farms considering wind characteristics," *IEEE Trans. Energy Convers.*, vol. 37, no. 1, pp. 631–642, Mar. 2022.

[10] M. P. Bahrman, "HVDC transmission overview," in *Proc. IEEE/PES Transmiss. Distrib. Conf. Expo.*, 2008, pp. 1–7.

[11] O. Gomis-Bellmunt, J. Sau-Bassols, E. Prieto-Araujo, and M. Cheah-Mane, "Flexible converters for meshed HVDC grids: From flexible AC transmission systems (FACTS) to flexible DC grids," *IEEE Trans. Power Del.*, vol. 35, no. 1, pp. 2–15, Feb. 2020.

[12] G. J. Kish and P. W. Lehn, "A comparison of modular multilevel energy conversion processes: DC/AC versus DC/DC," in *Proc. Int. Power Electron. Conf.*, 2014, pp. 951–958.

[13] W. Chen, A. Q. Huang, C. Li, G. Wang, and W. Gu, "Analysis and comparison of medium voltage high power DC/DC converters for offshore wind energy systems," *IEEE Trans. Power Electron.*, vol. 28, no. 4, pp. 2014–2023, Apr. 2013.

[14] M. Barrenetxea, I. Baraia, I. Larrazabal, I. Zubimendi, G. P. Adam, and B. W. Williams, "Analysis, comparison and selection of DC-DC converters for a novel modular energy conversion scheme for DC offshore wind farms," in *Proc. IEEE EUROCON - Int. Conf. Comput. Tool*, 2015, pp. 1–6.

[15] P. Hu, R. Yin, Z. He, and C. Wang, "A modular multiple DC transformer based DC transmission system for PMSG based offshore wind farm integration," *IEEE Access*, vol. 8, pp. 15736–15746, 2020.

[16] C. Sun, J. Zhang, G. Shi, and X. Cai, "Inter-arm phase-shift modulation scheme for isolated modular multilevel DC-DC converter," in *Proc. IEEE 8th Int. Power Electron. Motion Control Conf.*, 2016, pp. 53–58.

[17] S. Jafarishiadeh, V. Dargahi, A. K. Sadigh, and M. Farasat, "Novel multiterminal MMC-based DC/DC converter for MVDC grid interconnection," *IET Power Electron.*, vol. 11, no. 7, pp. 1266–1276, Jun. 2018.

[18] Y. Chen, Y. Cui, X. Wang, X. Wei, and Y. Kang, "Design and implementation of the low computational burden phase-shifted modulation for DC–DC modular multilevel converter," *IET Power Electron.*, vol. 9, no. 2, pp. 256–269, 2016.

[19] A. Schn and M. M. Bakran, "A new HVDC-DC converter for the efficient connection of HVDC networks," in *Proc. PCIM Europe Conf. Proc.*, 2013, pp. 525–832.

[20] W. Lin, "DC–DC Autotransformer with bidirectional DC fault isolating capability," *IEEE Trans. Power Electron.*, vol. 31, no. 8, pp. 5400–5410, Aug. 2016.

[21] G. J. Kish, M. Ranjram, and P. W. Lehn, "A modular multilevel DC/DC converter with fault blocking capability for HVDC interconnects," *IEEE Trans. Power Electron.*, vol. 30, no. 1, pp. 148–162, Jan. 2015.

[22] P. Klimczak, P. Blaszczyk, R. Jez, and K. Koska, "Double wye modular multilevel converter - Direct DC-DC topology," in *Proc. 8th IET Int. Conf. Power Electron., Mach. Drives*, 2016, pp. 1–6.

[23] S. Du, B. Wu, K. Tian, D. Xu, and N. R. Zargari, "A novel medium-voltage modular multilevel DC–DC converter," *IEEE Trans. Ind. Electron.*, vol. 63, no. 12, pp. 7939–7949, Dec. 2016.

[24] X. Zhao, B. Li, B. Zhang, and D. Xu, "A high-power step-up DC/DC converter dedicated to DC offshore wind farms," *IEEE Trans. Power Electron.*, vol. 37, no. 1, pp. 65–69, Jan. 2022.

[25] J. Liu et al., "A High step-up ratio DC-DC converter with fault blocking capability for offshore wind farms," in *Proc. IEEE 12th Energy Convers. Congr. Expo. - Asia*, 2021, pp. 702–707.

[26] J. Yang, Z. He, H. Pang, and G. Tang, "The hybrid-cascaded DC–DC converters suitable for HVdc applications," *IEEE Trans. Power Electron.*, vol. 30, no. 10, pp. 5358–5363, Oct. 2015.

[27] W. Chen, X. Ruan, H. Yan, and C. K. Tse, "DC/DC conversion systems consisting of multiple converter modules: Stability, control, and experimental verifications," *IEEE Trans. Power Electron.*, vol. 24, no. 6, pp. 1463–1474, Jun. 2009.

[28] T. Ishibashi, T. Jimichi, and Y. Sato, "Novel high-voltage high-power DC-DC converter for offshore wind farms," in *Proc. 20th Eur. Conf. Power Electron. Appl.*, 2018, pp. P.1–P.8.

[29] T. Lagier and P. Ladoux, "A comparison of insulated DC-DC converters for HVDC off-shore wind farms," in *Proc. Int. Conf. Clean Elect. Power*, 2015, pp. 33–39.

[30] H. Ding, G. Zou, F. Wang, and C. Xu, "Modelling and control strategies of DC offshore wind farm," in *Proc. 8th Asia Conf. Power Elect. Eng.*, 2023, pp. 1224–1228.

[31] X. Zhang, B. Cai, S. Yan, and C. Sun, "Current sharing control of non-isolated high power modular bi-directional DC/DC converter for HVDC-Flexible system in offshore wind farm," in *Proc. Chin. Automat. Congr.*, 2020, pp. 5256–5261.

[32] P. Hu, R. Yin, B. Wei, Y. Luo, and F. Blaabjerg, "Modular isolated LLC DC/DC conversion system for offshore wind farm collection and integration," *IEEE Trans. Emerg. Sel. Topics Power Electron.*, vol. 9, no. 6, pp. 6713–6725, Dec. 2021.

[33] S. Cui, N. Soltau, and R. W. D. Doncker, "A high step-up ratio soft-switching DC–DC converter for interconnection of MVDC and HVDC grids," *IEEE Trans. Power Electron.*, vol. 33, no. 4, pp. 2986–3001, Apr. 2018.

[34] Y. Qiao, X. Zhang, X. Xiang, X. Yang, and T. C. Green, "Trapezoidal current modulation for bidirectional high-step-ratio modular DC–DC converters," *IEEE Trans. Power Electron.*, vol. 35, no. 4, pp. 3402–3415, Apr. 2020.

[35] X. Xiang, X. Zhang, Y. Zhu, G. P. Chaffey, Y. Gu, and T. C. Green, "The resonant modular multilevel DC converters for high step-ratio and low step-ratio interconnection in MVDC distribution network," in *Proc. IECON - 45th Annu. Conf. IEEE Ind. Electron. Soc.*, 2019, pp. 5686–5693.

[36] X. Zhang, M. Tian, X. Xiang, J. Pereda, T. C. Green, and X. Yang, "Large step ratio input-series–output-parallel chain-link DC–DC converter," *IEEE Trans. Power Electron.*, vol. 34, no. 5, pp. 4125–4136, May 2019.

[37] Y. Shi and H. Li, "Isolated modular multilevel DC–DC converter with DC fault current control capability based on current-fed dual active bridge for MVDC application," *IEEE Trans. Power Electron.*, vol. 33, no. 3, pp. 2145–2161, Mar. 2018.

[38] S. Cui, N. Soltau, and R. W. D. Doncker, "Dynamic performance and fault-tolerant capability of a TLC-MMC hybrid DC-DC converter for interconnection of MVDC and HVDC grids," in *Proc. IEEE Energy Convers. Congr. Expo.*, 2017, pp. 1622–1628.

[39] I. A. Gowaid, G. P. Adam, S. Ahmed, D. Holliday, and B. W. Williams, "Analysis and design of a modular multilevel converter with trapezoidal modulation for medium and high voltage DC-DC transformers," *IEEE Trans. Power Electron.*, vol. 30, no. 10, pp. 5439–5457, Oct. 2015.

[40] P. Li, G. P. Adam, S. J. Finney, and D. Holliday, "Operation analysis of thyristor-based front-to-front active-forced-commutated bridge DC transformer in LCC and VSC hybrid HVDC networks," *IEEE Trans. Emerg. Sel. Topics Power Electron.*, vol. 5, no. 4, pp. 1657–1669, Dec. 2017.

[41] I. A. Gowaid, G. P. Adam, A. M. Massoud, S. Ahmed, D. Holliday, and B. W. Williams, "Quasi two-level operation of modular multilevel converter for use in a high-power DC transformer with DC fault isolation capability," *IEEE Trans. Power Electron.*, vol. 30, no. 1, pp. 108–123, Jan. 2015.

[42] H.-J. Lee, J.-j. Jung, and S.-K. Sul, "A switching frequency reduction and a mitigation of voltage fluctuation of modular multilevel converter for HVDC," in *Proc. IEEE Energy Convers. Congr. Expo.*, 2014, pp. 483–490.
[43] A. Schoen, A. Birkel, and M. Bakran, "Modulation and losses of modular multilevel converters for HVDC applications," in *Proc. PCIM Europe; Int. Exhib. Conf. Power Electron., Intell. Motion, Renewable Energy Energy Manage.*, 2014, pp. 1–8.
[44] S. H. Kung and G. J. Kish, "A modular multilevel HVDC buck–boost converter derived from its switched-mode counterpart," *IEEE Trans. Power Del.*, vol. 33, no. 1, pp. 82–92, Feb. 2018.

Yanan Ye (Graduate Student Member, IEEE) received the B.S. degree in electrical engineering from the Beijing Institute of Technology, Beijing, China, in 2018. He is currently working toward the Ph.D. degree in electrical engineering with Xi'an Jiaotong University, Xi'an, China.

His research focuses on the design and control of dc–dc converters for the HVdc transmission.

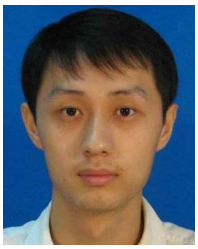

Xiaotian Zhang (Senior Member, IEEE) was born in Xi'an, China, in 1983. He received the B.S. (with Honors) and M.S. degrees in electrical engineering from Jiaotong University, Xi'an, China, in 2006 and 2009, respectively, and the Ph.D. degree (with Honors) in electrical engineering and electronics from the University of Liverpool, Liverpool, U.K., in 2012.

Until 2015, he was with the Department of Electrical Engineering, Imperial College London, London, U.K. He is currently an Associate Professor with the Department of Electrical Engineering, Xi'an Jiaotong University, Xi'an. His research focuses on the control and design of the HVdc converters.

Chong Gao (Student Member, IEEE) received the B.S. degree in electrical engineering from Qingdao University, Qingdao, China, in 2021. He is currently working toward the M.S. degree in electrical engineering from Xi'an Jiaotong University, Xi'an, China.

His research focuses on the design and control of dc–dc converters for HVdc transmission.

Xianwei Wang received the B.S. and Ph.D. degrees in electrical engineering from Xi'an Jiaotong University, Xi'an, China, in 2006 and 2013, respectively.

Since 2013, he has been an employee of Xi'an XJ Power Electronics Technology Company Ltd., Xi'an, where he is currently a Deputy General Manager. His research focuses on system analysis and design for HVdc system and medium voltage dc distribution system.

Yue Wang (Senior Member, IEEE) received the B.S. degree from Xi'an Jiaotong University, Xi'an, China, in 1993, the M.S. degree from Beijing Jiaotong University, Beijing, China, in 1999, and the Ph.D. degree from Xi'an Jiaotong University, in 2003, all in electrical engineering.

From 1993 to 1996, he was an Electrical Engineer with Xi'an Power Electronics Technology Research Institute, Xi'an. He is currently a Full Professor with the School of Electrical Engineering, Xi'an Jiaotong University. His research interests include wireless power transfer, active power filters, multilevel converters, and HVdc.

Xu Yang (Senior Member, IEEE) received the B.S. and Ph.D. degrees in electrical engineering from Xi'an Jiaotong University, Xi'an, China, in 1994 and 1999, respectively.

Since 1999, he has been a Member of the Faculty of School of Electrical Engineering, Xi'an Jiaotong University, where he is currently a Professor. From 2004 to 2005, he was with the Center of Power Electronics Systems, Virginia Polytechnic Institute and State University, Blacksburg, VA, USA, as a Visiting Scholar. He then came back to Xi'an Jiaotong University, and engaged in the teaching and research works in power electronics and industrial automation area. His research interests include soft switching topologies, PWM control techniques, power electronic integration, and packaging technologies.